International Journal of Engineering Research & Science (IJOER)
ISSN: [2395-6992]
[Vol-12, Issue-4, April- 2026]
Website: www.ijoer.com
Journal DOI: 10.25125/engineering-journal

# Effect of Rare-Earth Site Composition Complexity on the Microstructure and Mechanical Properties of High-Entropy $RE_3NbO_7$ Ceramics

Zongjian Yang[1*]; Xiaojun Yang[2]; Hui Li[3]; Peng Zhang[4]

School of Materials Science and Engineering, Beijing University of Technology, Beijing100124, China
*Corresponding Author

Received: 04 April 2026/ Revised: 13 April 2026/ Accepted: 22 April 2026/ Published: 30-04-2026


***Abstract—*** *High-entropy strategies provide a robust approach for tailoring the microstructural evolution and mechanical properties of ceramics. This study investigates the kinetic influence of rare-earth (RE) site compositional complexity on the phase stability, densification, and grain growth of $RE_3NbO_7$ ceramics. A series of compositions, from single-component $Sm_3NbO_7$ to a five-component (5RE) high-entropy system, were synthesized via solid-state reaction. X-ray diffraction confirms the formation of pure orthorhombic phases, characterized by distinct lattice distortions. Despite all compositions achieving high relative densities (>98%) at 1600°C, the increase in RE-site complexity profoundly suppressed grain growth. Notably, the 4RE composition exhibited the most pronounced grain refinement, reaching a minimum average grain size of 3.37μm (a 71% reduction compared to $Sm_3NbO_7$). This suppression is governed by a competitive mechanism between entropy-driven sluggish diffusion and the intrinsic physicochemical properties of the constituent elements. Mechanical evaluations reveal that the 4RE, 3RE, and 2RE compositions exhibit peak Vickers hardness (7.67GPa), fracture toughness (2.25 $MPa{\cdot}m^{1/2}$), and flexural strength (180MPa), respectively. These findings demonstrate that entropy-mediated design effectively decouples densification from grain coarsening and enables the systematic modulation of mechanical performance in niobate ceramics.*

***Keywords— High Entropy, Rare-earth Niobates, Composition Complexity, Densification, Mechanical Properties.***

## I. INTRODUCTION

Rare-earth niobates ($RE_3NbO_7$) have attracted significant research interest due to their structural diversity and exceptional high-temperature stability[1-5]. Depending on the $RE^{3+}$ ionic radius, these compounds typically crystallize into either cubic defect fluorite or orthorhombic weberite-type structures. To date, the high-entropy strategy has been extensively employed in the $RE_3NbO_7$ system to optimize various functional properties, such as achieving ultra-low thermal conductivity for thermal barrier coatings or tailoring magnetic behaviors for cryogenic magnetocaloric applications [6-9].

However, despite the proliferation of performance-oriented studies, the intrinsic kinetic influence of configurational entropy on the sintering process remains insufficiently understood. In the processing of advanced ceramics, achieving high densification often triggers rapid grain coarsening, which may lead to microstructural instability and degraded mechanical reliability. Although the sluggish diffusion effect is considered a hallmark of high-entropy systems, its quantitative impact on grain boundary mobility within the complex orthorhombic lattice of $RE_3NbO_7$ has not been systematically investigated. Most existing literature focuses on the final physical properties, whereas the fundamental evolution from single-component to multi-component compositions, and how this entropy escalation governs grain refinement is often overshadowed[10, 11].

In this work, we deliberately shift the focus from functional metrics to the fundamental relationship between RE-site complexity and microstructural evolution. By synthesizing a series of compositions ranging from single-component $Sm_3NbO_7$ to a five-component (5RE) high-entropy system via a solid-state reaction method, we isolate the effect of chemical disorder on densification behavior and grain growth inhibition. Through X-ray diffraction and scanning electron microscopy, we elucidate

the competitive mechanism between lattice strain and kinetic retardation. This study aims to provide a mechanistic framework for the precision microstructural control of niobate ceramics, establishing a necessary foundation for the future design of high-stability rare-earth niobates independent of specific performance targets.

## II. MATERIAL AND METHODS

### 2.1 Material design and Synthesis

The raw materials used in this study included high-purity oxide powders: $La_2O_3$, $Nd_2O_3$, $Sm_2O_3$, $Eu_2O_3$, $Gd_2O_3$, and $Nb_2O_5$ (all with 99.9% purity on a metals basis). A series of niobate ceramics, including $Sm_3NbO_7$, $(La_{0.5}Gd_{0.5})_3NbO_7$ (2RE), $(La_{1/3}Sm_{1/3}Gd_{1/3})_3NbO_7$ (3RE), $(Nd_{0.25}Sm_{0.25}Eu_{0.25}Gd_{0.25})_3NbO_7$ (4RE), and $(La_{1/5}Nd_{1/5}Sm_{1/5}Eu_{1/5}Gd_{1/5})_3NbO_7$ (5RE), were synthesized by solid-state reaction. The powders were pre-dried and stoichiometrically weighed and homogenized in anhydrous ethanol via planetary ball milling (zirconia ball, 250 rpm, 400 min). After removing the solvent via rotary evaporation and drying at 100 °C for 1 h, the precursor powders were calcined in a muffle furnace at 900 °C for 5 h. The calcined powders were then crushed, sieved through a 200-mesh screen, and subjected to a second ball-milling step for an extended duration of 800 min under identical conditions.

Following subsequent drying and sieving, the powders were granulated using a 5 wt% polyvinyl alcohol (PVA) aqueous solution (1.4 mL per 10 g of powder) and uniaxially pressed into φ14 mm green bodies. Binder burnout was conducted at 560 °C for 2 h with a slow heating rate of 1 °C/min. Ultimately, the pellets were sintered in a high-temperature furnace at 1600 °C for 10 h, followed by natural furnace cooling to room temperature.

### 2.2 Sample Preparation and Characterization

The samples were ground to achieve a flat surface and subsequently cleaned using an ultrasonic cleaner. The phase composition and crystal structure were characterized by X-ray diffraction (XRD). For microstructure observation, the surfaces were polished and thermally etched in a muffle furnace at 50 °C below the sintering temperature for 30 minutes. The surface morphology was then analyzed using scanning electron microscopy (SEM). The porosity of the samples was quantified from SEM images using ImageJ software, from which the relative density was determined.

## III. RESULT AND DISCUSSION

### 3.1 Phase Composition and Crystal Structure Analysis

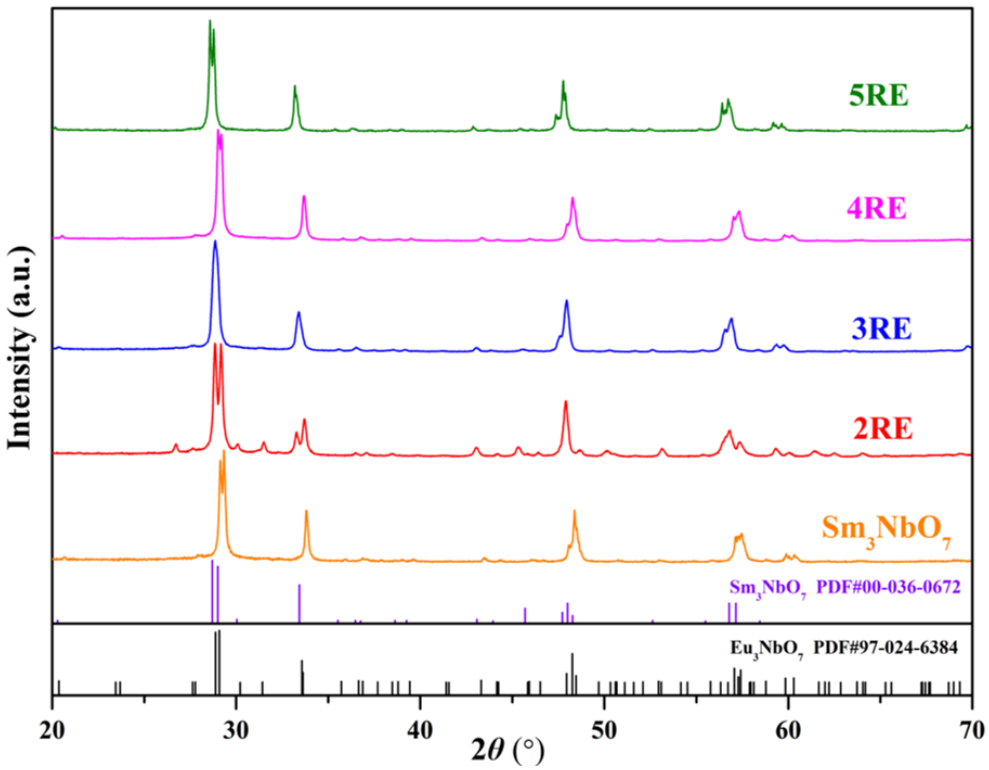


**FIGURE 1: The XRD pattern of $RE_3NbO_7$ ceramics sintered at 1600 °C**

The phase composition and crystalline evolution of the synthesized $RE_3NbO_7$ ceramics, ranging from single-component to five-component high-entropy systems, were characterized via X-ray diffraction (XRD). As illustrated in Figure 1, all samples exhibit well-defined diffraction profiles with high relative intensities, which can be perfectly indexed to a pure orthorhombic phase. No detectable secondary phases or residual precursors were observed, confirming that the rare-earth ions have been successfully incorporated into a single-phase host lattice to form a stabilized crystal structure via the solid-state reaction.

Detailed structural analysis via whole-pattern fitting (WPF) reveals a distinct transition in crystallographic symmetry as a function of RE-site complexity. The $Sm_3NbO_7$ and multi-component compositions (3RE, 4RE, and 5RE) crystallize into the $C222_1$ space group, while the 2RE composition maintains Cmcm symmetry[12]. Notably, a characteristic splitting of the diffraction peaks (doublet) at approximately $2\theta \approx 29$ ° is clearly observed in the 2RE sample. However, as the configurational entropy increases—accompanied by a decrease in lanthanum (La) content—these doublets gradually attenuate and merge into monolithic reflections. This phenomenon signifies a localized "lattice averaging" effect induced by the high-entropy strategy, where the significant size mismatch and chemical disorder among the multiple RE-site cations intensify the lattice distortion within the weberite framework[13].

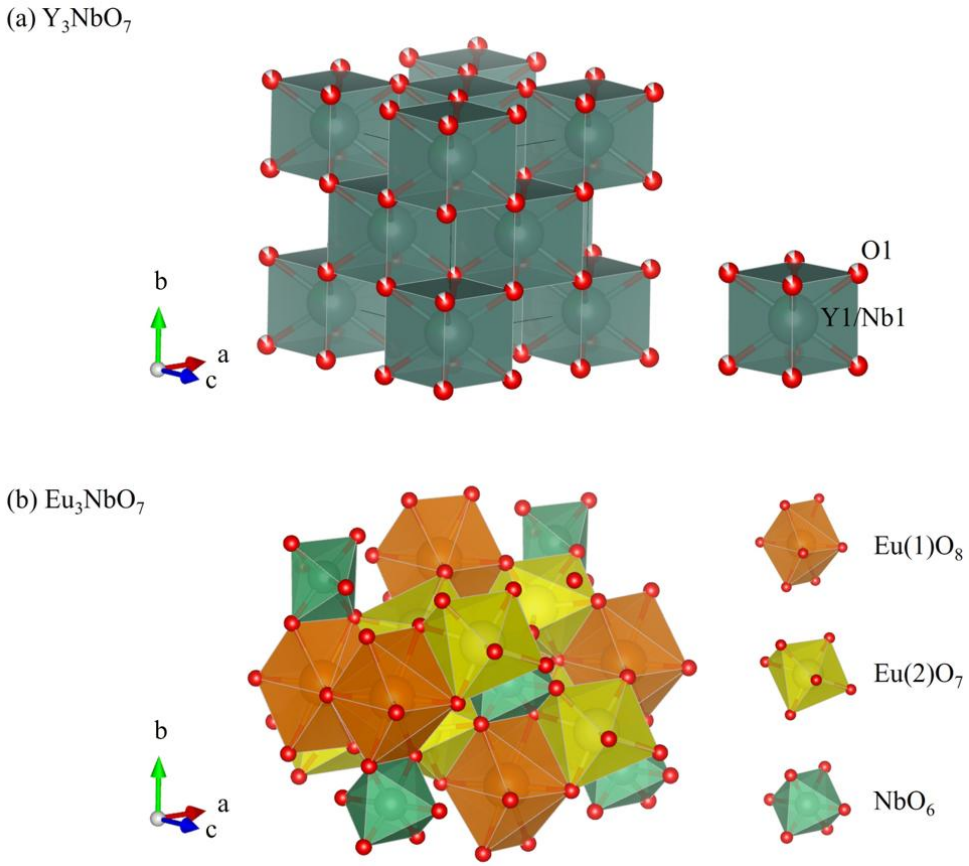


**FIGURE 2: Crystal structures of $RE_3NbO_7$ ceramics crystallizing in (a) defect fluorite and (b) weberite structures**

The structural features of the $RE_3NbO_7$ system are further elucidated by the atomic models presented in Figure 2. $Y_3NbO_7$ is shown as a representative of the defect fluorite structure for $RE_3NbO_7$ with smaller $RE^{3+}$ ions. In the high-symmetry defect fluorite structure, cations (Y/Nb) and oxygen vacancies are randomly distributed over their respective crystallographic sites, forming a uniform cubic framework[14]. Conversely, the orthorhombic weberite structure($Eu_3NbO_7$) represents a lower-symmetry variant characterized by the long-range ordering of three distinct cation polyhedra: $Eu(1)O_8$, $Eu(2)O_7$, and $NbO_6$[15]. The $NbO_6$ octahedra are predominantly linked via corner-sharing, while the larger rare-earth polyhedra occupy the interstitial sites, connecting to the framework through a combination of edge- and corner-sharing modes.

The crystallographic parameters summarized in Table 1 confirm the orthorhombic nature of these unit cells ($\alpha=\beta=\gamma= 90°$). Based on the fitted data, the lattice constants exhibit a geometric relationship of $a \approx 2^{1/2}b$ (e.g., for $Sm_3NbO_7$, $10.70/7.54 \approx 1.42$), which is a structural hallmark of weberite-type niobates derived from a parent fluorite lattice[16]. To quantify the effect of compositional complexity, the systematic evolution of the unit cell volume($V_C$) was analyzed. As summarized in Table 1, the

unit cell volume ($V_C$) exhibits a synergistic fluctuation with the average ionic radius ($\bar{r}_{RE}$), confirming the successful incorporation of multiple $RE^{3+}$ cations into the weberite lattice.

**TABLE 1**
**THE CELL PARAMETERS, FORMULA UNITS ($Z$), UNIT CELL VOLUME (VC), CONFIGURATIONAL ENTROPY ($S_{conf}$), AVERAGE IONIC RADIUS ($\bar{r}_{RE}$), RELIABILITY FACTOR (R), LATTICE DISTORTION DEGREE ($\delta$), AND RELATIVE DENSITES ($\rho_r$) OF $RE_3NbO_7$ CERAMICS SINTERED AT 1600 ℃**

| Composition | $Sm_3NbO_7$ | 2RE | 3RE | 4RE | 5RE |
|---|---|---|---|---|---|
| a (Å) | 10.7029 | 10.8721 | 10.7448 | 10.6928 | 10.7294 |
| b (Å) | 7.53901 | 7.5279 | 7.5737 | 7.5445 | 7.5768 |
| c (Å) | 7.6172 | 7.6551 | 7.6289 | 7.6134 | 7.6562 |
| α=β=γ (°) | 90 | 90 | 90 | 90 | 90 |
| $Z$ | 4 | 4 | 4 | 4 | 4 |
| $V_C$ (Å$^3$) | 614.6 | 626.5 | 620.8 | 614.2 | 622.4 |
| $S_{conf}$ (R) | 0 | 0.6931R | 1.1065R | 1.3863R | 1.6094R |
| $\bar{r}_{RE}$ (Å) | 1. 079 | 1. 1065 | 1.0973 | 1.0768 | 1.0934 |
| $R$ | 16.19% | 10.88% | 15.41% | 9.00% | 12.07% |
| $\delta$ | - | 4.84% | 4.15% | 1.93% | 3.49% |
| $\rho_r$（%） | 99.96 | 99.99 | 98.9 | 99.6 | 99.55 |

### 3.2 Sintering Behavior and Microstructural Evolution

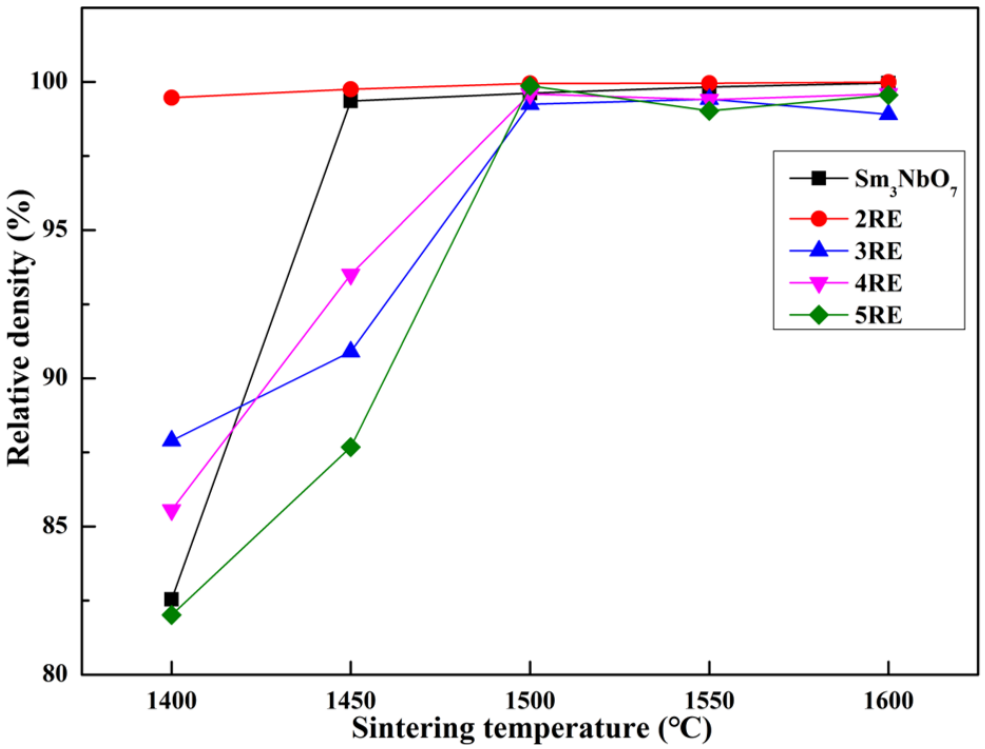


**FIGURE 3: The relative density of $RE_3NbO_7$ ceramics sintered at 1400 ℃-1600 ℃**

The densification behavior of the $RE_3NbO_7$ ceramics as a function of sintering temperature is depicted in Figure 3. It is evident that the relative density of all compositions increases monotonically as the temperature rises from 1400 °C to 1600 °C, reflecting a progressive elimination of porosity and a clear densification trend. Notably, the 2RE sample maintains a superiority

in densification across all tested temperatures, reaches a maximum relative density of 99.99% at 1600 °C (Table 1). While the 3RE and 5RE samples exhibit relatively lower densification rates at intermediate temperatures, all compositions ultimately achieve a high relative density exceeding 98% upon reaching 1600 °C. This indicates that the high-entropy strategy, despite increasing the chemical complexity, does not significantly impede the final stages of macroscopic densification.

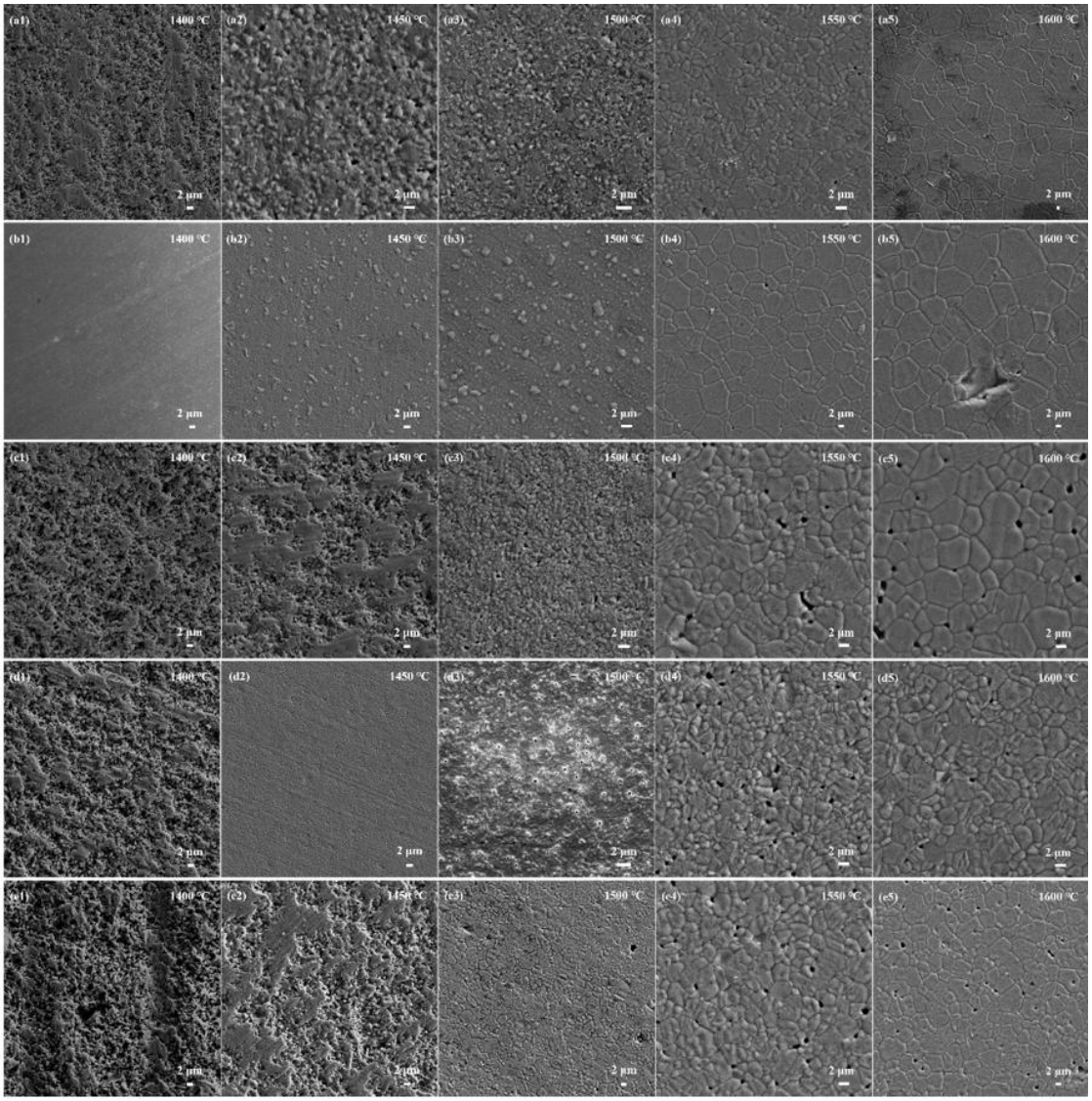


**FIGURE 4: The SEM images of $RE_3NbO_7$ ceramics sintered at 1400 ℃-1600 ℃: (a1-a5) $Sm_3NbO_7$; (b1-b5) 2RE; (c1-c5) 3RE; (d1-d5) 4RE; (e1-e5) 5RE**

The evolution of surface morphology, as captured by SEM in Figure 4, illustrates the transition from a highly porous state to a dense structure with well-defined grain boundaries as the temperature increases. However, a critical observation is the profound impact of RE-site complexity on the grain growth kinetics.

At lower sintering temperatures (1400 °C to 1500 °C), the samples exhibit nascent stages of sintering. These microstructures are characterized by an abundance of interconnected porosity and fine, indistinct particulates. It is evident that at these temperatures, the driving force for mass transport is insufficient to overcome the energy barriers for grain boundary formation, particularly in the multi-component systems. For the 4RE and 5RE compositions, the surfaces at 1450 °C and 1500 °C remain relatively flat or exhibit a "nanocrystalline" appearance, suggesting that high configurational entropy significantly shifts the densification window toward higher temperatures.

As the sintering temperature increases to 1550°C and 1600 °C, the microstructures undergo a dramatic transformation. Porosity is largely eliminated, and the ceramics develop well-defined, equiaxed grains with clearly delineated boundaries. This indicates the completion of the final stage of sintering, where grain growth kinetics become the dominant microstructural process.

A comparative analysis of the samples sintered at 1600 °C highlights the impact of compositional complexity on grain growth. The binary $Sm_3NbO_7$ and the 2RE ceramics exhibit the coarsest grains, whereas the 4RE sample demonstrates the most pronounced grain refinement. This suppression of grain growth at elevated temperatures further corroborates the sluggish diffusion effect in high-entropy ceramic systems. The multiple rare-earth cations create a complex local environment that hinders long-range diffusion, thereby stabilizing the fine-grained structure even at 1600 °C. However, all compositions achieve a high degree of compactness at this terminal temperature, confirming that 1600 °C is an optimal sintering temperature for achieving dense $RE_3NbO_7$ high-entropy ceramics with controlled microstructural features.

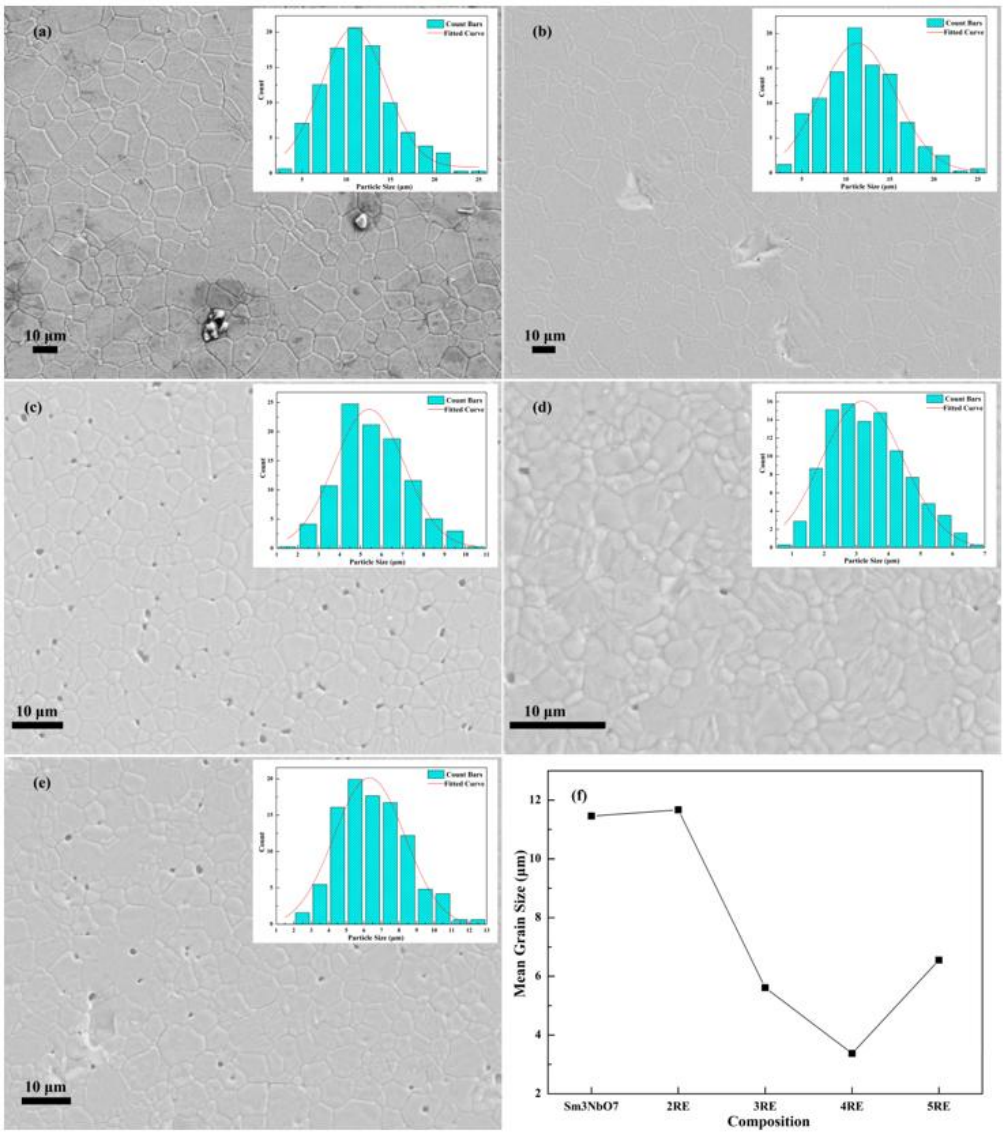


**FIGURE 5: Microstructural morphology and grain size analysis of $RE_3NbO_7$ ceramics: (a-e) SEM images of the samples with corresponding grain size distribution histograms (insets); (f) Variation of the mean grain size as a function of the sample composition.**

The surface morphologies and corresponding grain size distributions of the sintered ceramics are illustrated in Figure 5 (a–e). All specimens exhibit a highly densified microstructure characterized by well-defined grain boundaries and predominantly equiaxed grain morphologies. Negligible residual porosity is observed at the triple junctions, indicating that the selected sintering parameters were sufficient for achieving near-theoretical density.

The statistical analysis of grain size, depicted in the inset histograms of Figure 5 (a–e), reveals that the grain populations for all compositions conform well to a Gaussian distribution. For the $Sm_3NbO_7$ and 2RE samples, the distributions are relatively broad, with grain sizes spanning a wide range from approximately 5 µm to 25 µm. As the configurational entropy increases with the addition of more rare-earth elements, a significant shift in the distribution is observed. In the 3RE and 4RE samples,

the distribution curves markedly narrow and migrate toward the lower end of the scale, representing a high degree of microstructural refinement and homogeneity. However, for the 5RE composition, the distribution breadth slightly increases again, suggesting a moderate variation in grain growth kinetics.

As shown in Figure 5 (f), the average grain size varies significantly with compositional complexity. Compared to the $Sm_3NbO_7$ reference (11.46 μm), the 2RE composition shows a slight increase, reaching a peak of 11.67 μm. Remarkably, a dramatic non-monotonic reduction in grain size occurs as the system transitions to higher entropy states. The multi-component high-entropy strategy effectively suppresses grain growth compared to the near-single-component references. Among all compositions, the 4RE sample displays the most significant grain refinement, achieving a minimum average grain size of 3.37 μm at 1600 °C. This substantial reduction is a direct manifestation of the sluggish diffusion effect inherent in high-entropy systems. To further elucidate this mechanism, the lattice distortion degree ($\delta$) based on the atomic radii mismatch was considered[17]. Interestingly, the calculated $\delta$ for the 4RE system ($\delta$ = 1.93%) is lower than that of the 2RE system ($\delta$ = 4.84%), yet 4RE exhibits the strongest grain growth inhibition. This anomaly suggests that in the $RE_3NbO_7$ weberite framework, kinetic retardation is driven less by simple ionic radius mismatch and more by the intense chemical disorder and the cocktail effect of the four equimolar cations (Nd, Sm, Eu, Gd). The uniform distribution of chemically distinct cations maximizes the fluctuation of local bonding energies, thereby significantly elevating the activation energy barrier for grain boundary migration[18].

In the 5RE composition, the grain size undergoes a moderate recovery to 6.55 μm, although it remains considerably finer than that of the $Sm_3NbO_7$ reference. This microstructural recovery can be fundamentally ascribed to an intricate interplay between the entropy-induced kinetic retardation and localized perturbations in atomic mobility. The introduction of the larger $La^{3+}$ cation in the 5RE system increases the unit cell volume which may partially alleviate local strain fields or alter the defect chemistry, thereby slightly lowering the energy barrier for atomic diffusion compared to the more compactly disordered 4RE lattice[19]. Furthermore, this phenomenon underscores that microstructural evolution during high-temperature sintering is not exclusively dictated by macroscopic configurational entropy. The intrinsic physicochemical properties of the constituent elements, such as variations in metal-oxygen bond strength, intrinsic atomic diffusivity, and surface energy among the diverse $RE^{3+}$ cations, play a critical role in governing local mass transport. Consequently, the specific elemental characteristics within the 5RE system may introduce localized diffusion pathways that partially offset the entropy-driven kinetic retardation. These results demonstrate the efficacy of the high-entropy effect in suppressing grain coarsening while maintaining high density, providing critical insights for the microstructural engineering of advanced rare-earth niobate ceramics.

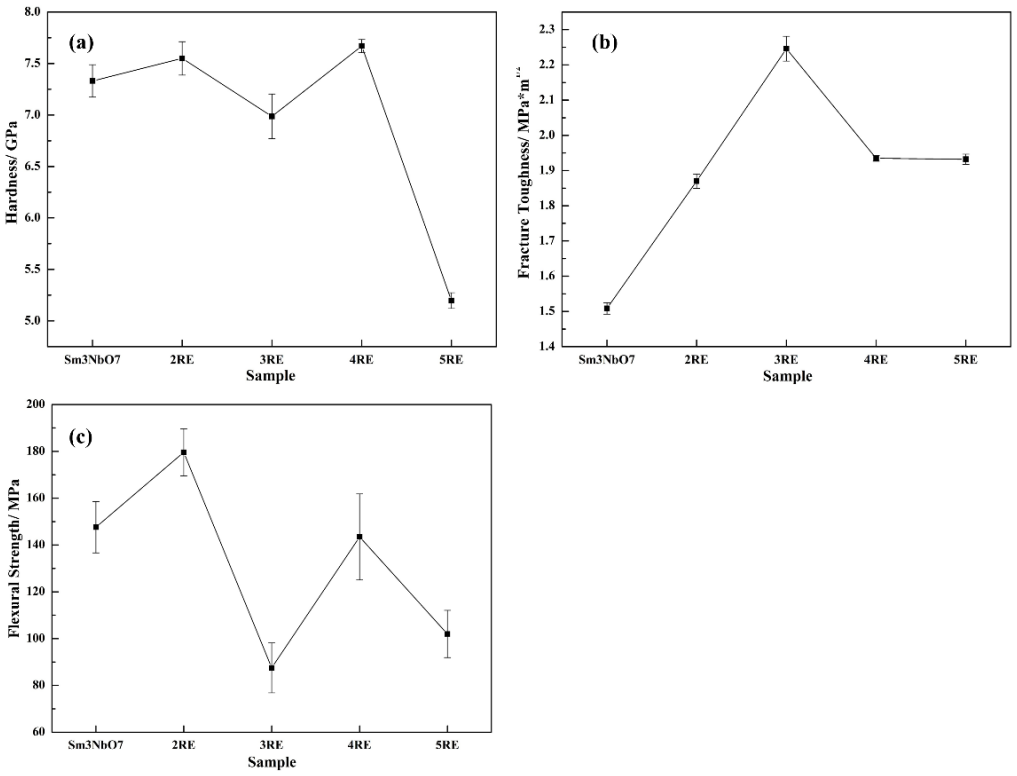


**FIGURE 6: Mechanical properties of the $RE_3NbO_7$ ceramics sintered at 1600 °C as a function of the sample composition: (a) Vickers hardness; (b) Flexural strength; and (c) Fracture toughness**

The mechanical properties of the sintered $RE_3NbO_7$ ceramics, including Vickers hardness, fracture toughness, and flexural strength, are illustrated in Figure 6. The results demonstrate a complex dependence of mechanical performance on the configurational entropy and compositional complexity of the rare-earth sublattice.

The Vickers hardness of the specimens as a function of composition is presented in Figure 6 (a). The hardness of the base $Sm_3NbO_7$ sample is 7.33 ± 0.15 GPa. With the initial substitution of rare-earth elements, the hardness increases to a peak value of 7.67 ± 0.05 GPa for the 4RE composition. This enhancement is primarily attributed to solid solution strengthening and the high-entropy effect, where the significant atomic size mismatch between the various rare-earth cations induces localized lattice strain, effectively pinning dislocations and resisting plastic deformation during indentation. Notably, a precipitous decline to 5.20 ± 0.06 GPa is observed for the 5RE sample. Such a sharp decrease suggests that excessive lattice distortion or a potential transition in the chemical bonding environment may lead to a reduction in the cohesive energy of the lattice, thereby compromising the intrinsic hardness[20, 21].

The variation in fracture toughness is shown in Figure 6 (b). A clear upward trend is observed from the $Sm_3NbO_7$ sample (1.51 ± 0.02 $MPa{\cdot}m^{1/2}$) to the 3RE sample, which achieves a maximum toughness of 2.25 ± 0.03 $MPa{\cdot}m^{1/2}$. This represents a substantial enhancement of approximately 49% compared to the binary counterpart. This toughening behavior is closely correlated with the microstructural refinement observed in the SEM analysis; the significantly reduced grain size in the multi-component systems increases the grain boundary density, promoting energy-dissipating mechanisms such as crack deflection and crack branching[22]. For the 4RE and 5RE samples, the toughness stabilizes at approximately 1.93 $MPa{\cdot}m^{1/2}$, indicating that the toughening effect reaches a plateau as the grain size and lattice strain reach a critical balance.

Figure 6 (c) depicts the flexural strength of the ceramics. The strength exhibits a non-monotonic evolution, reaching its maximum in the 2RE composition (180 ± 10 MPa). A distinct dip is observed for the 3RE sample (87 ± 11 MPa), followed by a recovery in the 4RE sample (144 ± 18 MPa). The fluctuations in flexural strength are likely a result of the competition between grain refinement strengthening and the accumulation of internal residual stresses caused by the multi-component substitution[23]. While the 4RE sample exhibits the finest grain size, the 2RE system appears to maintain a superior balance between microstructural homogeneity and minimized lattice-induced micro-strains, resulting in the highest load-bearing capacity before catastrophic failure. The relatively small error bars across the measurements confirm the high densification and phase uniformity achieved during the sintering process.

## IV. CONCLUSION

In summary, this study systematically investigated the influence of rare-earth (RE) site compositional complexity on the phase stability and microstructural evolution of $RE_3NbO_7$ ceramics

1. All synthesized compositions formed phase-pure orthorhombic structures and achieved high relative densities exceeding 98% at 1600 °C, with the 2RE sample exhibiting the highest densification rate.

2. Increasing the configurational entropy exerted a profound, non-monotonic suppression on grain growth. The 4RE composition exhibited the most significant grain refinement, achieving a minimum average grain size of 3.37 μm, a substantial reduction compared to the $Sm_3NbO_7$ (11.46 μm)

3. This deep suppression is attributed to the sluggish diffusion effect and chemical disorder induced by the multi-cation framework. Although a moderate size recovery (6.55 μm) was observed in the 5RE system due to competitive lattice strain, it remained considerably finer than the low-entropy reference.

4. The mechanical properties of $RE_3NbO_7$ ceramics are significantly modulated by compositional complexity. Specifically, the 4RE composition maximizes Vickers hardness at 7.67 GPa through solid solution strengthening, while the 3RE sample achieves peak fracture toughness (2.25 $MPa{\cdot}m^{1/2}$, a 49% increase) via grain refinement and crack deflection. Conversely, the 2RE system exhibits the highest flexural strength (180 MPa), attributed to an optimal balance between microstructural homogeneity and minimized lattice micro-strain.

These findings demonstrate that strategically tailoring RE-site complexity is a highly effective approach for decoupling densification from grain growth, offering a robust kinetic framework for the microstructural engineering of advanced niobate ceramics.

## CONFLICT OF INTEREST

The authors declare no conflict of interest.

## REFERENCES

[1] Chen, L., Hu, M., Wu, P., & Feng, J. (2019). Thermo-mechanical properties of fluorite Yb3TaO7 and Yb3NbO7 ceramics with glass-like thermal conductivity.
[2] Hinatsu, Y., & Doi, Y. (2017). Studies on phase transition temperature of rare earth niobates Ln3NbO7 (Ln = Pr, Sm, Eu) with orthorhombic fluorite-related structure.
[3] Chen, L., Hu, M., Wu, P., & Feng, J. (2020). Features of crystal structures and thermo-mechanical properties of weberites RE3NbO7 (RE = La, Nd, Sm, Eu, Gd) ceramics.
[4] Chen, L., Song, P., & Feng, J. (2018). Potential thermal barrier coating materials: RE3NbO7 (RE = La, Nd, Sm, Eu, Gd, Dy) ceramics.
[5] Yang, J., Qian, X., Pan, W., & Wan, C. (2019). Mechanical properties, oxygen barrier property, and chemical stability of RE3NbO7 for thermal barrier coating.
[6] Xiang, H., Xing, Y., Dai, F., Wang, H., Su, L., Miao, L., Zhang, G., Wang, Y., Qi, X., Yao, L., & Zhou, Y. (2021). High-entropy ceramics: Present status, challenges, and a look forward.
[7] Zhu, J., Meng, X., Xu, J., Ma, Y., & Zhang, P. (2021). Ultra-low thermal conductivity and enhanced mechanical properties of high-entropy rare earth niobates (RE3NbO7, RE = Dy, Y, Ho, Er, Yb).
[8] Ma, X., Liu, Y., & Wen, W. (2025). Thermophysical properties and CMAS corrosion behavior of high-entropy RE3NbO7-type rare-earth niobate ceramic.
[9] Chen, F., Wang, H., Li, Y., & Liu, Y. (2025). Structural and magnetic characterization of weberite-type RE3NbO7 (RE = Gd, Dy, Ho, and Er) ceramics with notable cryogenic magnetocaloric responses.
[10] Cao, J., Liu, X., Wang, Y., & Chen, L. (2024). Synthesis and thermal behavior of rare-earth-niobate ceramics with fluorite structure.
[11] Xiang, S., Li, Z., Zhao, Y., & Zhang, H. (2026). Thermophysical and mechanical modulation of RE3NbO7 ceramics via compositional entropy design.
[12] Bao, J., Zhang, Z., Li, E., & Yue, Z. (2022). Crystal structures, bond characteristics, and dielectric properties of novel middle-εr Ln3NbO7 (Ln = Nd, Sm) microwave dielectric ceramics with opposite temperature coefficients.
[13] Yang, X., Liu, B., & Wang, H. (2025). Preparation and properties of high-entropy rare earth niobate LnNbO4 microwave dielectric ceramics.
[14] Imer, M. R., Suescun, L., & Rabuffetti, F. A. (2023). A small-box approach to the local crystal structure of Y3NbO7.
[15] Liu, L., Xu, D., Zhang, H., & Li, E. (2021). Eu3NbO7: Novel middle-dielectric constant microwave dielectric ceramic with monoclinic structure.
[16] Qin, M., Gild, J., Wang, H., & Luo, J. (2022). 21-Component compositionally complex ceramics: Discovery of ultrahigh-entropy weberite and fergusonite phases and a pyrochlore-weberite transition.
[17] Zhu, J., Gao, S., Liu, J., & Yang, G. (2021). Enhanced mechanical and thermal properties of ferroelastic high-entropy rare-earth-niobates.
[18] Zhang, W., Chen, L., & Xu, C. (2022). Grain growth kinetics and densification mechanism of (TiZrHfVNbTa)C high-entropy ceramic under pressureless sintering.
[19] Zhou, L., Li, F., Liu, J. X., & Zhang, G. J. (2023). Fast grain growth phenomenon in high-entropy ceramics: A case study in rare-earth hexaaluminates.
[20] Brewer, L. (1977). The cohesive energies of the elements.
[21] Yao, G., Liu, J. X., Xu, Q., & Zhang, G. J. (2022). Local orders, lattice distortions, and electronic structure dominated mechanical properties of (ZrHfTaM1M2)C (M = Nb, Ti, V).
[22] Han, Y., Liang, B., Lu, Y., & Wang, Y. (2022). In-situ synthesis of gadolinium niobate quasi-binary composites with balanced mechanical and thermal properties for thermal barrier coatings.
[23] Hassan, R., & [Additional authors if available]. (2025). Flexural strength of (Hf,Nb,Ta,Ti,Zr)B2-(Hf,Nb,Ta,Ti,Zr)C high-entropy dual-phase ceramics.